Inorganic Chemistry

ARTICLE

pubs.acs.org/IC

Syntheses and Characterization of New Mid-Infrared Transparency Compounds: Centric Ba_2BiGaS_5 and Acentric Ba_2BiInS_5

Lei Geng,[†,‡] Wen-Dan Cheng,*[,†] Chen-Sheng Lin,[†] Wei-Long Zhang,[†] Hao Zhang,[†] and Zhang-Zhen He[†]

[†]State Key Laboratory of Structural Chemistry, Fujian Institute of Research on the Structure of Matter, Chinese Academy of Sciences, Fuzhou 350002, People's Republic of China

[‡]Graduate School of the Chinese Academy of Sciences, Beijing 100039, People's Republic of China

Supporting Information

ABSTRACT: Two new mid-infrared transparency compounds, centric Ba_2BiGaS_5 (**1**) and acentric Ba_2BiInS_5 (**2**), were synthesized from a high-temperature solid-state reaction in evacuated closed silica tubes. Their crystal structures were determined by a single crystal X-ray diffraction method at 293 K. The results of crystal structure solution indicate that compound **1** crystallizes in the centrosymmetric space group *Pnma* with *trans*-$_1^\infty[BiGaS_5]^{4-}$ chain structure, while compound **2** crystallizes in the noncentrosymmetric polar space group $Cmc2_1$ with *cis*-$_1^\infty[BiInS_5]^{4-}$ chain structure. Two types of lone-pair electrons alignment fashions within $_1^\infty[BiMS_5]^{4-}$ chains result in destructive (for **1**) or constructive (for **2**) dipole moments, as illustrated in the crystal structures and the partial electron density maps based on the first-principles electronic structure computations. Powder second-harmonic generation (SHG) experiments with a 2.05 μm pumping laser show that the SHG efficiency of the polar compound **2** is approximately 0.8 times that of $KTiOPO_4$ (KTP) reference. Furthermore, SHG signal intensity measurements using different size particles of powder samples indicate that compound **2** can also achieve type I phase-matching, which makes the compound promising for practical applications.

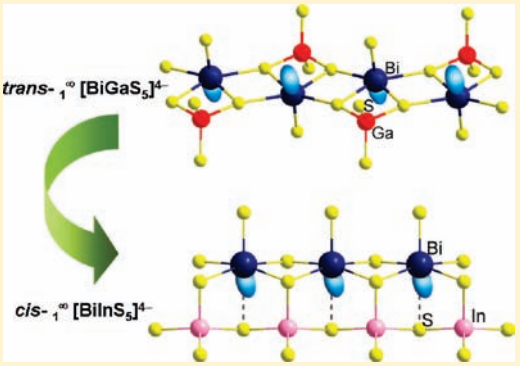

INTRODUCTION

Mid-infrared (mid-IR, 2−25 μm) light sources are of great interest for many applications from molecular spectroscopy and frequency metrology to communication, laser surgery, gas monitoring, and sensing. Coherent mid-IR radiation generation from nonlinear optical (NLO) crystals is one of the most significant ways, as efficient mid-IR laser materials and technologies are less maturely developed currently.[1,2] At present, the remarkable nonlinear materials made of oxides, such as β-BaB_2O_4 (BBO), LiB_3O_5 (LBO), and $KTiOPO_4$ (KTP), are widely applied from the ultraviolet to near-IR spectral range.[3−7] In the mid-IR region, however, there are only a few NLO crystals such as $AgGaS_2$, $AgGaSe_2$, and $ZnGeP_2$ can be commercially available so far. Moreover, relatively high mid-IR optical absorption and low laser damage threshold in these materials obstructs further improvement of the laser power.[8−10] In addition, these marked NLO materials have no wide transparency in the mid-IR region, and their IR transparency cutoff edge is commonly less than about 20 μm. Accordingly, it is particularly meaningful to exploit new NLO materials with a wide range of mid-IR transparency as well as large NLO susceptibility.

Second-order NLO behavior, that is, second harmonic generation (SHG), if the Kleinman's symmetry and phase-matching conditions are not considered, can exist in the 20 acentric crystal classes except for class 432 (O).[11,12] In order to obtain acentric crystal structure and large microscopic second-order NLO susceptibility, several strategies have been employed. For instance, π-conjucted planar anionic groups (such as trigonal-planar BO_3^{3-} and BS_3^{3-} units, B: boron) are able to produce large birefringence and strong electron polarization,[3−5,13,14] and stereochemically active lone-pair cations (Sb^{3+}, Se^{4+}, Te^{4+}, I^{5+}, etc.) or d^0 configured transition metals (Ti^{4+}, V^{5+}, Nb^{5+}, Mo^{6+}, W^{6+}, etc.) are susceptible to second-order Jahn−Teller effects and result in asymmetric coordination environments.[15−25] In recent years, continuous research on chalcogenides has resulted in the discoveries of several new potential infrared NLO materials such as $LiGaS(e)_2$,[26] $LiInS(e)_2$,[27,28] $BaGa_4S(e)_7$,[29−31] $AgGaGeS_4$,[32−34] $LiGaGeS_4$,[35] $LiAsS_2$,[36] $AZrPSe_6$ (A = K, Rb, Cs),[37] $Cs_5BiP_4Se_{12}$,[38] and $K_2Hg_3Ge_2S_8$.[39] However, the crystallization of compounds with noncentrosymmetric space group arrangements seems difficult to be accurately predicted and designed, although approaches such as combining acentric units (e.g., tetrahedral GeS_4^{4-} anions) with heavy metals were reported to increase the odds of forming acentric structures.[11,39] In this work, we attempted to investigate on the Ba-Bi-M-S (M = Ga, In) systems which combine the heavy metal Bi atoms with the MS_4 tetrahedra and thus may produce new crystal structures.

Received: March 3, 2011
Published: May 19, 2011

dx.doi.org/10.1021/ic2004358 | *Inorg. Chem.* 2011, 50, 5679–5686

Table 1. Crystal Data and Structure Refinement Results for Ba_2BiMS_5 (M = Ga, In)

empirical formula	Ba_2BiGaS_5	Ba_2BiInS_5
f.w.	713.68	758.78
T (K)	293(2)	293(2)
wavelength (Å)	0.71073	0.71073
crystal system	orthorhombic	orthorhombic
space group	*Pnma* (No. 62)	$Cmc2_1$ (No. 36)
a	12.180(6)	4.2535(17)
b	8.926(5)	18.252(7)
c	8.927(5)	12.685(5)
V (Å^3), Z	970.5(9), 4	984.8(7), 4
ρ_{calc} (g cm^{-3})	4.885	5.118
μ (mm^{-1})	29.825	28.996
F(000)	1224	1296
θ ranges (deg)	$2.83 \le \theta \le 27.49$	$2.23 \le \theta \le 27.46$
transmission, T_{min}/T_{max}	0.3484/1.0000	0.0519/0.0977
R_1[a], wR_2[b] ($I > 2\sigma$)	0.0208, 0.0462	0.0361, 0.0773
R_1, wR_2 (all data)	0.0220, 0.0467	0.0380, 0.0778
GOF on F^2	1.137	1.019

[a] $R_1 = \Sigma||F_o| - |F_c||/\Sigma|F_o|$. [b] $wR_2(F_o^2) = [\Sigma w(F_o^2 - F_c^2)^2/\Sigma w(F_o^2)^2]^{1/2}$.

Intensive efforts led to the discoveries of two quaternary compounds, Ba_2BiGaS_5 (**1**) with centrosymmetrc (CS) *Pnma* space group structure and Ba_2BiInS_5 (**2**) with noncentrosymmetric (NCS) $Cmc2_1$ space group structure. In this paper, we will report the syntheses by a high-temperature solid-state method in evacuated silica tubes, structure determination by a single crystal X-ray diffraction method, and the optical properties of the two compounds. In particular, powder SHG measurements show that compound **2** exhibits large SHG efficiency, which is similar to that of a powder KTP reference. Moreover, first-principles calculations based on density functional theory (DFT) were carried out in order to better understand the relationships between crystal structures and optical properties for the title compounds.

EXPERIMENTAL SECTION

Synthesis. The following reagents were used without further purification: BaS (99.7%, Alfa), Bi (99.999%, Sinopharm Chemical Reagent Co., SCRC), Ga (99.999%, SCRC), In (99.999%, SCRC), S (99.5%, SCRC). Compound **1** were prepared by a solid-state reaction method from stoichiometric amounts of BaS (0.2848 g, 1.682 mmol), Bi (0.1757 g, 0.841 mmol), Ga (0.0586 g, 0.841 mmol), and S (0.0809 g, 2.523 mmol). The starting materials were well mixed and loaded into a graphite ampule which was subsequently placed into a predried silica tube and then sealed under 10^{-2} Pa. The above sample was placed into a vertical furnace and heated to 973 K within 30 h (holding for 30 h), subsequently heated to 1223 K at the rate of 10 K/h (holding for 30 h) and then slowly cooled down to room temperature at the rate of 2 K/h. Many light-yellow block-shaped single crystals, subsequently determined as Ba_2BiGaS_5, were produced in the ampule. Compound **2** was prepared by a solid-state reaction method from stoichiometric amounts of BaS (0.3572 g, 2.108 mmol), Bi (0.2203 g, 1.054 mmol), In (0.1211 g, 1.054 mmol), and S (0.1014 g, 3.162 mmol). The procedure of preparation and synthesis of compound **2** is similar to that of **1**. After the temperature decreased, a lot of black slab-shaped Ba_2BiInS_5 was produced. Both of the two compounds are stable in air and moisture conditions. X-ray energy dispersive spectroscopy (EDS, Oxford INCA) analysis on a field-emission scanning electron microscope (FESEM, JSM6700F) on each sample indicated an Ba/Bi/M/S molar ratio of 2.14:1.08:1.0:4.78 for M = Ga and 2.07:1.12:1.03:4.96 for M = In, which are in agreement with their stoichiometric proportions from the results of single-crystal X-ray structure analyses.

Table 2. Selected Bond Lengths (Å) for Ba_2BiMS_5 (M = Ga, In)

atom	distance	atom	distance
	Ba_2BiGaS_5		
Ba(1)−S(3)	3.2463(18)	Ba(1)−S(1)	3.4098(19)
Ba(1)−S(4)	3.2809(18)	Bi(1)−S(2)	2.526(2)
Ba(1)−S(2)	3.2820(18)	Bi(1)−S(1) × 2	2.6504(16)
Ba(1)−S(4)	3.2970(18)	Bi(1)−S(1) × 2	3.0756(19)
Ba(1)−S(1)	3.319(2)	Ga(1)−S(4)	2.219(2)
Ba(1)−S(2)	3.3317(18)	Ga(1)−S(3)	2.253(2)
Ba(1)−S(3)	3.3460(18)	Ga(1)−S(1) × 2	2.2999(16)
	Ba_2BiInS_5		
Ba(1)−S(2)	3.160(6)	Ba(2)−S(1)	3.638(7)
Ba(1)−S(5) × 2	3.203(4)	Bi(1)−S(4)	2.582(5)
Ba(1)−S(4) × 2	3.223(4)	Bi(1)−S(2) × 2	2.794(4)
Ba(1)−S(1)	3.304(7)	Bi(1)−S(3) × 2	2.959(4)
Ba(1)−S(3) × 2	3.399(4)	Bi(1)−S(1)	3.212(4)
Ba(2)−S(5) × 2	3.156(4)	In(1)−S(5)	2.447(6)
Ba(2)−S(2) × 2	3.219(4)	In(1)−S(1) × 2	2.501(4)
Ba(2)−S(4) × 2	3.229(4)	In(1)−S(3)	2.578(6)
Ba(2)−S(3)	3.476(6)		

Crystal Structure Determinations. A crystalline sample of **1** was selected for indexing and intensity data collection on a Rigaku Mini diffractometer equipped with graphite-monochromated Mo Kα radiation (λ = 0.71073 Å) at the temperature of 293 K, and a sample of **2** was measured on a Mercury CCD diffractometer equipped with graphite-monochromated Mo Kα radiation (λ = 0.71073 Å) at the temperature of 293 K. The Rigaku CrystalClear program was utilized for diffraction images collection and data procession. Lorentz and polarization corrections were also applied for data reduction. The crystal structures were solved by direct methods and refined by full-matrix least-squares on F^2 using SHELXL-97.[40] Systematic absence conditions of the data suggest their possible space groups which were used for further structure solution and refinement. The final refined solution was checked by using the program PLATON, and no other symmetry elements were suggested.[41] Crystallographic data and structural refinements information are summarized in Table 1. The atomic coordinates and equivalent isotropic displacement parameters are listed in Table S1, Supporting Information. The important bond lengths are shown in Table 2, and the angles are shown in Table S2, Supporting Information. Further details of the crystal structure investigations may be obtained from the Fachinformationszentrum Karlsruhe, 76344 Eggenstein-Leopoldshafen, Germany (fax: (+49)7247−808−666; e-mail: crysdata@fiz-karlsruhe.de) on quoting the depository numbers of CSD-422398 for Ba_2BiGaS_5 and CSD- 422399 for Ba_2BiInS_5.

Powder X-ray diffraction patterns were recorded at room temperature on a Rigaku MiniFlex II diffractometer equipped with Cu Kα radiation (λ = 1.5418 Å) for the two compounds. The scanning range is 5−65° in 2θ with a step size of 0.01° and exposure time of 0.3 s. The measured powder XRD patterns are in good agreement with the calculated ones based on their single crystal structures, as shown in Figures S1a for **1** and S1b for **2** in Supporting Information.

dx.doi.org/10.1021/ic2004358 |*Inorg. Chem.* 2011, 50, 5679–5686

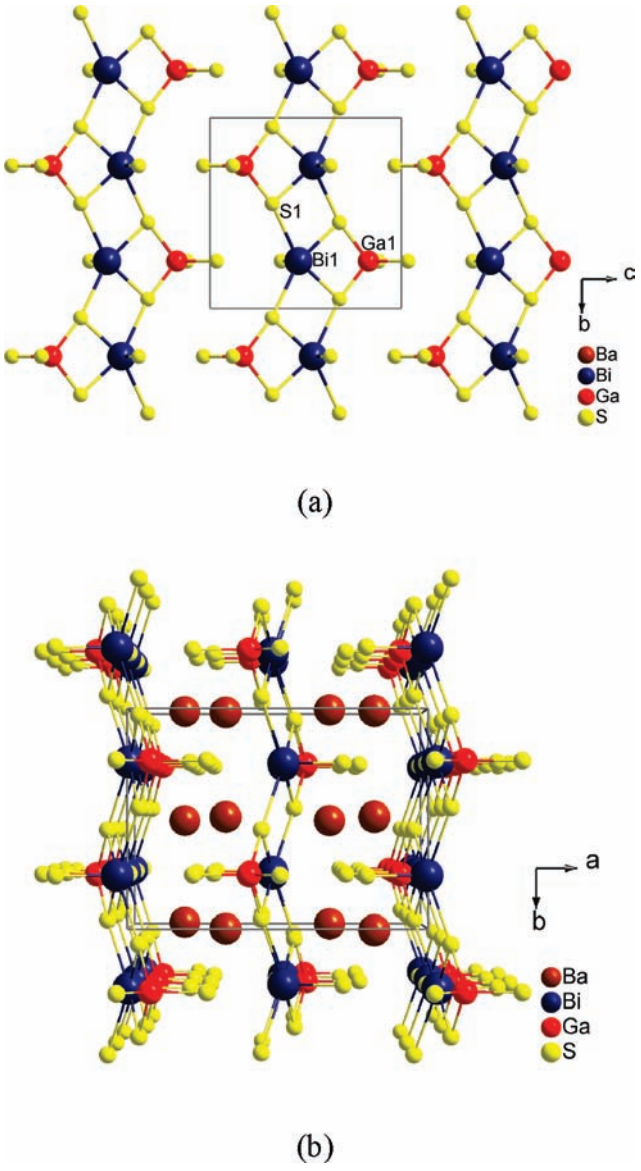

Figure 1. (a) The structural fragment of $_1^{\infty}[BiGaS_5]^{4-}$ anionic chains in compound Ba_2BiGaS_5 and (b) the whole crystal architecture viewed down the *c*-axis.

Optical Properties Measurements. The infrared spectra of compounds **1** and **2** were recorded on a PerkinElmer Spectrum One FT-IR spectrometer in the range of 450−7000 cm^{-1} for the samples diluted with dry KBr and pressed into a thin pellet. The UV−vis-NIR diffuse reflectance spectrum was carried out on a PerkinElmer Lambda 900 UV−vis-NIR spectrometer equipped with an integrating sphere over a 300−2000 nm wavelength range at room temperature. A $BaSO_4$ plate was used as a reference material (100% reflectance). The optical absorption spectra were converted from diffuse reflectance spectra using the Kubelka−Munk function, $\alpha/S = (1 - R)^2/2R$, where *R* is the diffuse reflectance, α and *S* are the Kubelka−Munk absorption and scattering coefficients.[42]

As compound **2** crystallizes in the NCS $Cmc2_1$ polar space group, we measured the powder SHG efficiency to investigate its nonlinear properties by means of the Kurtz-Perry method.[43] Powder samples of **2** were ground and sieved into six distinct groups based on their particle sizes from 30 to 200 μm. Each sample with an amount of about 60 mg was pressed into a pellet and then irradiated with a 2.05 μm *Q*-switched laser. A filter was used to separate the 1.025 μm SHG signal from the fundamental wave. Powder KTP sample with particle sizes about 200 μm was used as a standard reference upon which the SHG intensities of **2** were calculated for all the measurements.

Computational Details. First-principles electronic structure calculations were performed in order to better comprehend the relationship between the optical property and the electronic structure for compounds **1** and **2**. The electronic energy band structure and density of state (DOS) calculations were performed by using the first-principles quantum mechanical program *CASTEP* within the DFT formalism.[44] The crystallographic data of compound **1** and **2** determined by X-ray single crystal diffraction were used without further geometry optimizations in the calculations. The interactions between valence electrons and ion cores were described by the norm-conserving pseudopotential.[45] Pseudo atomic calculations were performed for Ba $5s^25p^66s^2$, Ga $3d^{10}4s^24p^1$, In $5s^25p^1$, Bi $5d^{10}6s^26p^3$, and S $3s^23p^4$. Perdew−Burke−Ernzerhof (PBE) exchange-correlation function within the generalized gradient approximation (GGA) scheme was utilized in the total energy calculations.[46] The Monkhorst-Pack *k*-point grid samplings of 3 × 4 × 4 for **1** and 9 × 9 × 3 for **2** were applied in the DFT calculations.[47] Energy cutoff of 550 eV was used to determine the plane waves basis set. The other parameters used in the calculations were set by the default values of the *CASTEP* code.

RESULTS AND DISCUSSION

Structure Description. Compound **1** crystallizes in the orthorhombic space group *Pnma*, with *a* = 12.180(6) Å, *b* = 8.926(5) Å, *c* = 8.927(5) Å, and *Z* = 4. It is isostructural with our previously synthesized quaternary antiferromagnetic compound Ba_2BiFeS_5[48] and can be obtained by completely substituting Ga^{3+} for Fe^{3+} with the crystal structure unchanged. The basic structural unit of compound **1** is an infinite one-dimensional (1D) $_1^{\infty}[BiGaS_5]^{4-}$ anionic chain, which is composed of a BiS_5 tetragonal-pyramid chain with GaS_4 tetrahedra alternately connected on both sides of the BiS_5 polyhedral chain via edge-sharing (Figure 1a). These paralleled $_1^{\infty}[BiGaS_5]^{4-}$ anionic chains engage with each other along the *c*-axis direction and form the two-dimensional Bi−Ga−S layer perpendicular to the *a*-axis. Neighboring Bi−Ga−S layers further interpenetrate each other with the isolated Ba^{2+} cations arranged between layers for electric charge balances, constituting the whole crystal architecture (Figure 1b).

There is one Ba site, that is, Ba(1), at a general position (8d) in terms of Wyckoff notation in compound **1**. The Ba(1) atom is coordinated by eight nearest S atoms with bond lengths from 3.247(2) to 3.410(2) Å. Unlike Ba(1), the Bi(1) and Ga(1) atoms are both located on a symmetry plane, so their numbers are only half of the Ba atom in the compound formula. The 5-fold coordination polyhedron of the Bi^{3+} cation in the asymmetric unit is a distorted tetragonal pyramid with three short bond lengths of 2.526(2)−2.650(2) Å and two longer ones of 3.076(2) Å. The Bi atom moves considerably away from the bottom of the distorted BiS_5 pyramid due to the electron-repulsion effect from the stereoactive lone pair on Bi^{3+} cation with the bonding electron pairs on the next neighboring $S^{2-}(3)$ anion (Figure S2, Supporting Information). The Ga atom features a nonideal tetrahedral coordination geometry with S atoms with bond lengths of 2.219(2)−2.300(2) Å. Bond valence sum (BVS) calculations performed on Ba^{2+}, Bi^{3+}, and Ga^{3+} also give consistent values, as expected from their structural formula (Table S2, Supporting Information).[49,50]

dx.doi.org/10.1021/ic2004358 |*Inorg. Chem.* 2011, 50, 5679–5686

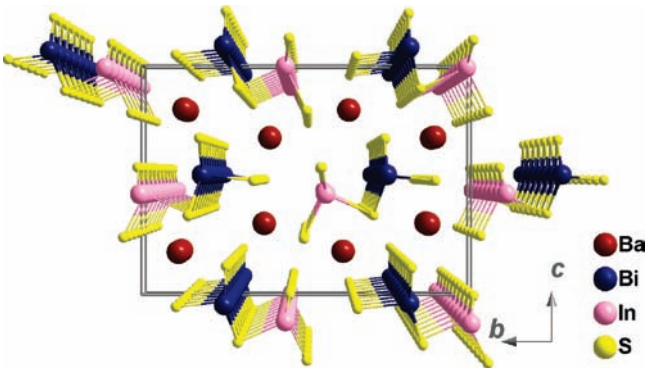

Figure 2. Crystal structure of compound Ba_2BiInS_5 viewed along the [100] direction.

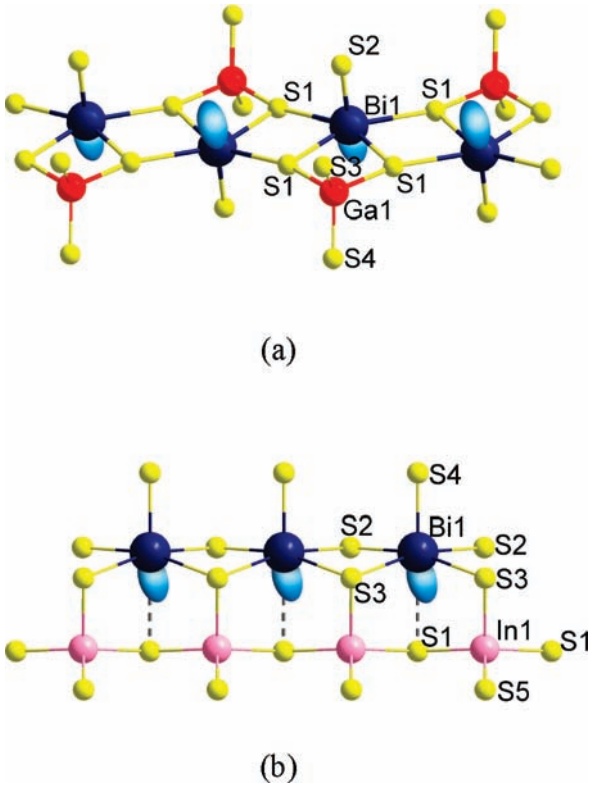

Figure 3. (a) 1D $_1^{\infty}[BiGaS_5]^{4-}$ chain in compound Ba_2BiGaS_5, and (b) 1D $_1^{\infty}[BiInS_5]^{4-}$ chain in compound Ba_2BiInS_5. The blue lobes on Bi atoms represent the lone pairs.

Compound **2** crystallizes in the orthorhombic space group $Cmc2_1$, with $a = 4.2535(17)$ Å, $b = 18.252(7)$ Å, $c = 12.685(5)$ Å, and $Z = 4$. The crystal structure consists of 1D $_1^{\infty}[BiInS_5]^{4-}$ anionic polymeric chains with charge-compensating Ba^{2+} ions arranged in six arrays around each $_1^{\infty}[BiInS_5]^{4-}$ chain along the crystallographic *a*-axis as shown in Figure 2. The $_1^{\infty}[BiInS_5]^{4-}$ chain is built up of an edge-shared BiS_5 tetragonal-pyramid chain and a corner-shared InS_4 tetrahedra chain, and the two kinds of chains are further interconnected with each other through sharing corner to form the whole $_1^{\infty}[BiInS_5]^{4-}$ anionic chain.

There are two crystallographically nonequivalent barium atoms, one bismuth atom, one indium atom, and five sulfur atoms in the asymmetric unit. The two symmetrically nonequivalent Ba^{2+}

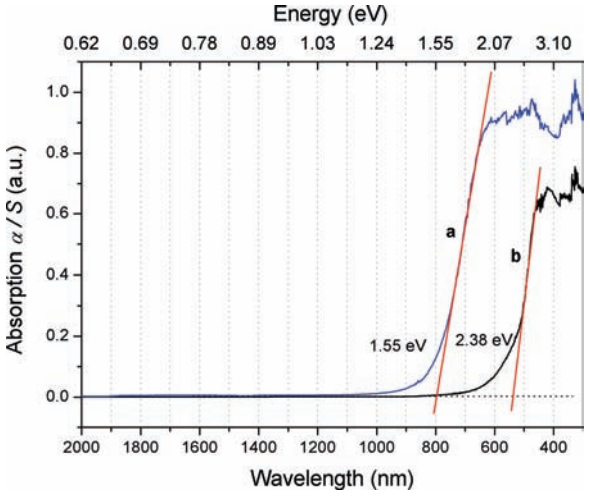

Figure 4. UV−vis-NIR optical absorption spectra converted from diffuse-reflectance spectra using the Kubelka−Munk equation for polycrystalline samples of (a) compound Ba_2BiGaS_5 and (b) compound Ba_2BiInS_5.

cations in Ba_2BiInS_5 are both coordinated by eight S atoms with bond lengths in the range of 3.160(6)−3.399(4) Å for Ba(1) and 3.156(4)−3.638(7) Å for Ba(2). The bond lengths of Bi−S vary from 2.582(5) to 2.959(4) Å, featuring the irregular tetragonal-pyramid coordination geometry. Considering the next neighboring S(1) atoms with bond length 3.212(7) Å, a seriously distorted octahedron indicates completeness. The unique In^{3+} cation in the asymmetric unit is coordinated by four S atoms in the tetrahedral arrangement with bond lengths distorted from 2.447(6) to 2.578(6) Å, while the S−In−S angles range from 92.39(19)° for S(1)−In(1)−S(4) to 116.5(3)° for S(5)−In(1)−S(5). The calculated BVS of Ba^{2+}, Bi^{3+}, and In^{3+} cations are in reasonable agreement with their normal oxidation states, respectively (Table S2, Supporting Information). According to the bond valence values of Bi^{3+} ions, most of them are distributed over the three nearest and two next nearest S atoms, while the farther S(1) atom has less contribution on the BVS.

One of the most interesting features about the title compounds Ba_2BiMS_5 is that there is a change from CS nonpolar structure for M = Ga to NCS polar structure for M = In, along with two types of Bi^{3+} lone-pair electrons alignment fashions in the two compounds. For compound **1**, the BiS_5 tetragonal pyramids and neighboring GaS_4 tetrahedra are aligned through *trans* arrangement along the $_1^{\infty}[BiGaS_5]^{4-}$ chain with the apexes of BiS_5 pyramids reversed up and down alternately (Figure 3a). Therefore, compound **1** is constructed by the *trans*-$_1^{\infty}[BiGaS_5]^{4-}$ chain structure. This arrangement leads to the Bi^{3+} lone-pair electrons out of the alignment and the local dipole moments offset each other due to their opposite directions within the *trans*-$_1^{\infty}[BiGaS_5]^{4-}$ chains, resulting in the CS nonpolar structure of compound **1**. However, for compound **2** the BiS_5 tetragonal pyramids and neighboring InS_4 tetrahedra are aligned through *cis* arrangement through sharing edge to form the *cis*-$_1^{\infty}[BiInS_5]^{4-}$ chain structure (Figure 3b). This arrangement leads to the Bi^{3+} lone-pair electrons in the constructive alignment fashion within the *cis*-$_1^{\infty}[BiInS_5]^{4-}$ chain. As shown in Figure 2, the lone-pair electrons on the Bi^{3+} are pointing toward the [011] direction in one-half number of the $_1^{\infty}[BiInS_5]^{4-}$ chains and toward the $[0\bar{1}1]$ direction in the other half number of

dx.doi.org/10.1021/ic2004358 |*Inorg. Chem.* 2011, 50, 5679–5686

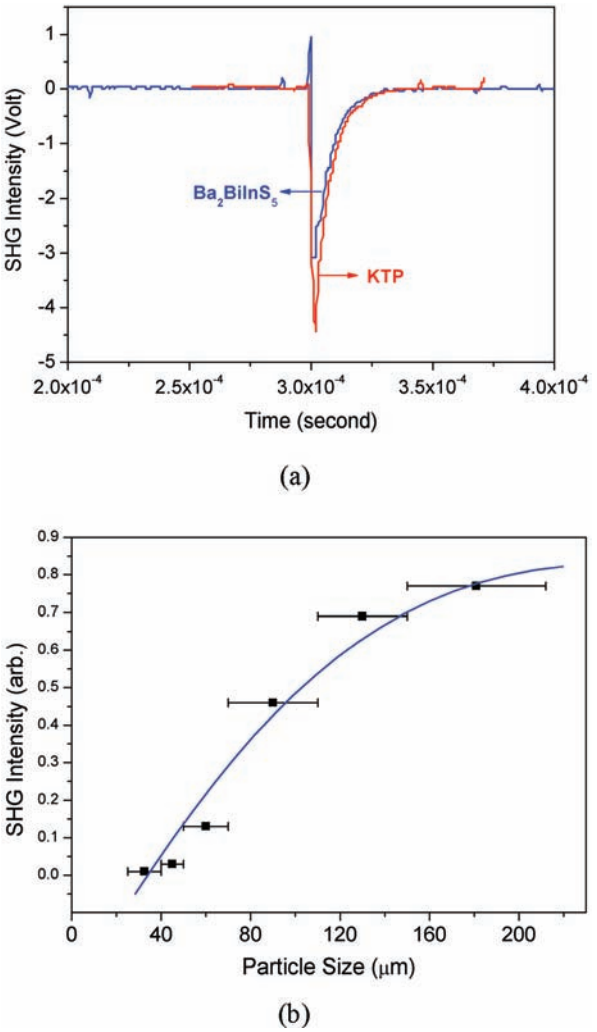

Figure 5. (a) The SHG intensity (blue line) of a Ba_2BiInS_5 sample compared with that (red line) of KTP, and (b) the SHG intensity against the different particle sizes of Ba_2BiInS_5 samples (blue line is for eye-guide).

the chains, and consequently the dipole moments will be destructive along the *b*-axis direction. But along the polar *c*-axis, there still remain some net dipole moments, which are believed to be mainly responsible for the SHG properties of compound **2**.

Thermal Analyses. Thermogravimetric (TGA) and differential thermal analysis (DTA) were performed simultaneously on a NETZSCH STA 449C thermal analyzer to investigate the thermal properties of the synthesized materials Ba_2BiGaS_5 and Ba_2BiInS_5. About 10 mg powder sample was placed into an Al_2O_3 crucible with the same one as reference and heated to 1200 at 10 °C/min in the N_2 atmosphere at a flow rate of 30 mL/min. TGA and DTA measurement results indicate that both compounds are thermally stable with almost no mass losses and no endo- or exothermeric peaks up to 800 °C under N_2 atmosphere (Figure S3, Supporting Information). From 850 to 1200 °C, about a 70% mass loss with several endothermic peaks was observed. This may be related to the decomposition of the compounds at high temperature over 850 °C.

Optical Properties. The IR spectra of polycrystalline **1** and **2** exhibit a wide infrared transmission range from near-IR up to 25 μm with no obvious optical absorption peaks (Figure S4,

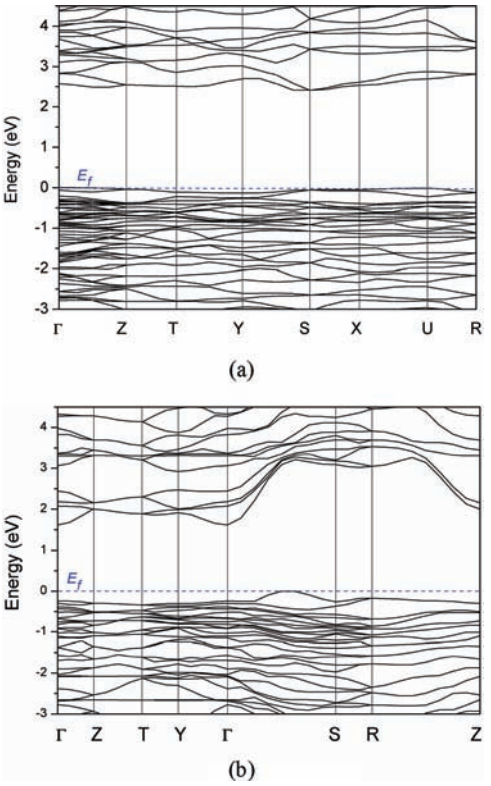

Figure 6. The band structures of (a) Ba_2BiGaS_5 and (b) Ba_2BiInS_5 in the ranges of −3.0 to 4.5 eV using the norm-conserving pseudopotential method. The Fermi level is set at 0 eV.

Supporting Information), which suggests that both compounds may be useful in the mid-IR and even to far-IR ranges. The UV−vis-NIR optical absorption spectra measurement results indicate that compounds **1** and **2** are both semiconductors with optical band gaps of about 2.38 and 1.55 eV, respectively (Figure 4).

For the NCS polar compound **2**, we have made NLO property investigations. The sieved powder samples of **2** were irradiated by using a 2.05 μm Q-switched laser and the SHG signal at 1.025 μm was detected. It revealed that the SHG signal is similar to (~0.8 times) that of the KTP standard with a similar grain size (~200 μm) at the incident wavelength of 2.05 μm (Figure 5a). From the plots of SHG signal intensity vs particle size of Ba_2BiInS_5 powders as shown in Figure 5b, it is found that for the particle size less than 120 μm, the SHG intensity increases gradually with increasing particle size, and for the particle size larger than 120 μm, the SHG intensity is essentially independent of particle size. This feature suggests that compound **2** can achieve type I phase-matching which makes compound **2** promising for practical applications.

Band Structures and DOSs. The calculated band structures along the special *k*-point in the first Brillouin zone (BZ) are plotted in Figure 6 for CS compound **1** and NCS polar compound **2**. The special *k*-point definitions and the corresponding state energies of the lowest conduction band and the highest valence band are listed in Table S3 in the Supporting Information. It is found from Figure 6a that the valence band maximum (VBM) is located at Γ point, and the conduction band minimum (CBM) is located at S point, indicating an indirect band gap of 2.41 eV for compound **1**, which is in agreement with the

dx.doi.org/10.1021/ic2004358 |*Inorg. Chem.* 2011, 50, 5679–5686

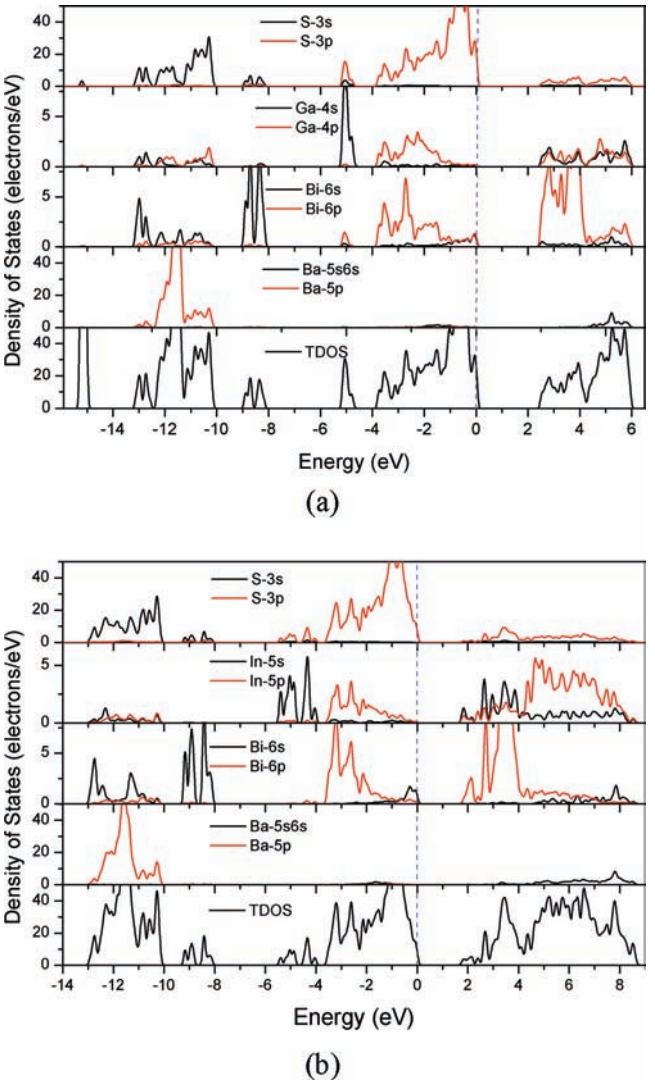

Figure 7. Total and partial density of states for compounds (a) Ba_2BiGaS_5 and (b) Ba_2BiInS_5 using the norm-conserving pseudopotential method.

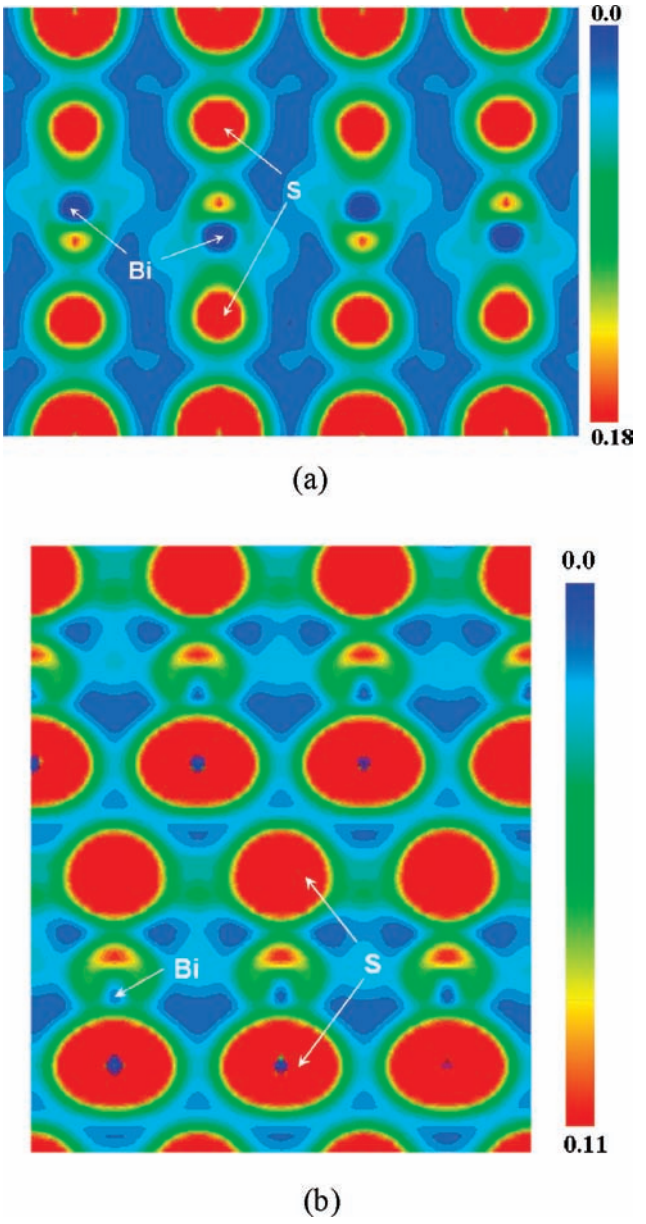

Figure 8. (a) PED maps for compound Ba_2BiGaS_5 from −2.5 eV to the Fermi level, and the electron density is represented from blue (0.0 e/Å^3) to red (0.18 e/Å^3). (b) PED maps for compound Ba_2BiInS_5 from −2.5 eV to the Fermi level, and the electron density is represented from blue (0.0 e/Å^3) to red (0.11 e/Å^3). The above DFT calculations were performed by using the PAW potential method.

measured one of 2.38 eV. From Figure 6b, the VBM is located at the middle of the ΓS line, while the CBM is located at the Γ point, indicating an indirect band gap of 1.61 eV for compound **2**, which is in agreement with the measured one of 1.55 eV.

The partial density of states (PDOS) and total density of states (TDOS) for the two compounds are plotted in Figure 7. It is found that the three bands are very sharp for the TDOS localized at between the energies of −28.0 eV and −13.0 eV. They are the contributions from the Ga 3d/In 4d, Bi 5d, and Ba 5s states and do not involve the covalent interaction in the investigated compounds. For both compounds, the highest occupied states ranging from −4.0 to 0.0 eV mainly contain S 3p states with small mixtures of Bi 6s6p and Ga 4s4p/In 5s5p states; the lowest unoccupied states from 2.4 eV (for **1**) or 1.6 eV (for **2**) to 6.5 eV strongly involve unoccupied Bi 6p states and less unoccupied Ga 4s4p/In 5s5p states. Thus, the charge transfers from occupied S 3p states to unoccupied Bi 6p states and hybridized Ga 4s4p or In 5s5p states are believed to make main contributions to the optical absorption for compounds **1** and **2**, respectively. From PDOS of Bi, we can see that the dominant contribution to Bi 6s is found at the lower energy range of −8.0 to −9.0 eV (for **1**) or −8.0 to −9.4 eV (for **2**), rather than at the top of the valence band, and that the indirect mixing between Bi 6s and Bi 6p states is mediated by hybridization with S 3p states at the top of valence band for both compounds. Moreover, it is worth pointing out that the hybridized states of Bi 6s with S 3p close to the Fermi level account for only a small fraction of the total Bi 6s states, but they play an important and crucial role in the formation of the Bi 6s lone pair. These findings show that the formation of the Bi^{3+} $6s^2$ lone pair has dependence on the S^{2-} anion, and this dependence on the electronic states of the anion can be evidence of the stereochemically active lone pair.[51,52]

dx.doi.org/10.1021/ic2004358 |*Inorg. Chem.* 2011, 50, 5679–5686

Partial Electron Density (PED). In order to visualize the Bi−S interactions in the specific regions of DOS, PED calculations were also performed for two title compounds by running the VASP software package.[53−55] The projector-augmented wave (PAW) potentials method was used in the PED calculations, and the other parameters set for VASP calculations are the same as those for CASTEP described in Computational Details. As expected, the results of the electronic structures and DOSs performed by the above two codes are identical. The PEDs for the states from −2.5 to 0.0 eV, that is, the Fermi level, were calculated for compounds **1** and **2**, respectively. The Ga 3d (In 4d), Bi 5d and Ba 5s states lie outside this range and play no significant roles in covalent interactions, and therefore, they have been excluded from the analyses. Two-dimensional electron density slices containing Bi and S atoms have been made through the (101) plane for **1** and through the (001) plane for **2**, respectively (Figure 8). An almost spherical electron distribution can be seen around the S atoms, while an asymmetric density distribution is clearly present around each Bi atom directed away from their nearest-neighboring S atom. This is an indication of the stereochemically active Bi^{3+} lone pairs. By comparison of Figure 8, panels a and b, we find that the stereochemically active Bi^{3+} lone pairs manifest different local dipole alignment fashions in two compounds. For compound **1**, these local dipole moments are in the opposite-direction alignment, and the cooperative effects of all local dipoles result in the offset of macroscopic dipole moments. For compound **2**, the local dipole moments are in parallel-direction alignment, and the cooperative effects of all local dipoles result in the enhancement of macroscopic dipole moments. This is also one of the reasons why the latter compound has large SHG responses.

CONCLUSIONS

In summary, two new compounds: centric Ba_2BiGaS_5 and acentric Ba_2BiInS_5 with excellent mid-infrared transparency have been synthesized, and the crystal structures have been determined to be space group *Pnma* with CS nonpolar structure for **1** and $Cmc2_1$ with NCS polar structure for **2**, respectively. A change from CS nonpolar to NCS polar structures results from different types of Bi^{3+} lone-pair electrons alignment fashions for two compounds. The calculated DOS and PED maps show that the Bi^{3+} lone pair is stereochemically active and the charge transfers from occupied S 3p states to unoccupied Bi 6p states and hybridized Ga 4s4p or In 5s5p states make the main contributions to the optical absorption for compounds **1** and **2**, respectively. Large SHG responses of polar material **2** are attributed to the parallel alignment of the local dipole moments induced from the Bi^{3+} lone pairs. The capability of achieving type I phase-matching makes compound **2** a potential candidate for nonlinear material used in mid-IR region.

ASSOCIATED CONTENT

Supporting Information. X-ray crystallographic files (CIF), table of selected bond lengths and BVS, simulated and experimental powder XRD patterns, and definitions of the special *k* points in the first BZ for Ba_2BiMS_5 (M = Ga, In). This material is available free of charge via the Internet at http://pubs.acs.org.

AUTHOR INFORMATION

Corresponding Author
*E-mail: cwd@fjirsm.ac.cn.

ACKNOWLEDGMENT

Authors wish to acknowledge the National Natural Science Foundation of China under Project 20773131, the National Basic Research Program of China (No. 2007CB815307), the Knowledge Innovation Program of the Chinese Academy of Sciences, and the Fujian Key Laboratory of Theory and Computational Chemistry for providing computation resources.

REFERENCES

(1) Majid, E.-Z.; Irina, T. S. *Mid-infrared Coherent Sources and Applications*; Springer: Dordrecht, Netherlands, 2005.
(2) Godard, A. *C. R. Phys.* **2007**, *8*, 1100–1128.
(3) Chen, C. T.; Wu, B. C.; Jiang, A. D.; You, G. M. *Sci. Sin., Ser. B* **1985**, *28*, 235–243.
(4) Chen, C. T.; Wu, Y. C.; Jiang, A. D.; Wu, B. C.; You, G. M.; Li, R. K.; Lin, S. J. *J. Opt. Soc. Am. B* **1989**, *6*, 616–621.
(5) Becker, P. *Adv. Mater.* **1998**, *10*, 979–992.
(6) Hagerman, M. E.; Poeppelmeier, K. R. *Chem. Mater.* **1995**, *7*, 602–621.
(7) Bierlein, J. D.; Vanherzeele, H. *J. Opt. Soc. Am. B* **1989**, *6*, 622–633.
(8) Harasaki, A.; Kato, K. *Jpn. J. Appl. Phys.* **1997**, *36*, 700–703.
(9) Eckardt, R. C.; Fan, Y. X.; Byer, R. L.; Marquardt, C. L.; Storm, M. E.; Esterowitz, L. *Appl. Phys. Lett.* **1986**, *49*, 608–610.
(10) Peterson, R. D.; Schepler, K. L.; Brown, J. L.; Schunemann, P. G. *J. Opt. Soc. Am. B* **1995**, *12*, 2142–2146.
(11) Halasyamani, P. S.; Poeppelmeier, K. R. *Chem. Mater.* **1998**, *10*, 2753–2769.
(12) Boyd, R. W. *Nonlinear Optics*; Academic Press: San Diega, 2003.
(13) Kim, Y.; Martin, S. W.; Ok, K. M.; Halasyamani, P. S. *Chem. Mater.* **2005**, *17*, 2046–2051.
(14) Geng, L.; Cheng, W. D.; Zhang, W. L.; Lin, C. S.; Zhang, H.; Li, Y. Y.; He, Z. Z. *Inorg. Chem.* **2010**, *49*, 6609–6615.
(15) Kim, M. K.; Kim, S. H.; Chang, H. Y.; Halasyamani, P. S.; Ok, K. M. *Inorg. Chem.* **2010**, *49*, 7028–7034.
(16) Kim, M. K.; Jo, V.; Lee, D. W.; Ok, K. M. *Dalton Trans.* **2010**, *39*, 6037–6042.
(17) Kunz, M.; Brown, I. D. *J. Solid State Chem.* **1995**, *115*, 395–406.
(18) Goodey, J.; Broussard, J.; Halasyamani, P. S. *Chem. Mater.* **2002**, *14*, 3174–3180.
(19) Ra, H. S.; Ok, K. M.; Halasyamani, P. S. *J. Am. Chem. Soc.* **2003**, *125*, 7764–7765.
(20) Halasyamani, P. S. *Chem. Mater.* **2004**, *16*, 3586–3592.
(21) Ok, K. M.; Halasyamani, P. S. *Angew. Chem., Int. Ed.* **2004**, *43*, 5489–5491.
(22) Jiang, H. L.; Huang, S. P.; Fan, Y.; Mao, J. G.; Cheng, W. D. *Chem.—Eur. J.* **2008**, *14*, 1972–1981.
(23) Mao, J. G.; Jiang, H. L.; Kong, F. *Inorg. Chem.* **2008**, *47*, 8498–8510.
(24) Li, P. X.; Kong, F.; Hu, C. L.; Zhao, N.; Mao, J. G. *Inorg. Chem.* **2010**, *49*, 5943–5952.
(25) Jo, V.; Kim, M. K.; Lee, D. W.; Shim, I. W.; Ok, K. M. *Inorg. Chem.* **2010**, *49*, 2990–2995.
(26) Isaenko, L.; Yelisseyev, A.; Lobanov, S.; Titov, A.; Petrov, V.; Zondy, J. J.; Krinitsin, P.; Merkulov, A.; Vedenyapin, V.; Smirnova, J. *Cryst. Res. Technol.* **2003**, *38*, 379–387.
(27) Isaenko, L.; Vasilyeva, I.; Yelisseyev, A.; Lobanov, S.; Malakhov, V.; Dovlitova, L.; Zondy, J. J.; Kavun, I. *J. Cryst. Growth* **2000**, *218*, 313–322.
(28) (a) Badikov, V. V.; Chizhikov, V. I.; Efimenko, V. V.; Efimenko, T. D.; Panyutin, V. L.; Shevyrdyaeva, G. S.; Scherbakov, S. I. *Opt. Mater.* **2003**, *23*, 575–581. (b) Isaenko, L.; Yelisseyev, A.; Lobanov, S.; Petrov, V.; Rotermund, F.; Slekys, G.; Zondy, J. J. *J. Appl. Phys.* **2002**, *91*, 9475–9480.
(29) Eisenmann, B.; Jakowski, M.; Schafer, H. *Rev. Chim. Miner.* **1983**, *20*, 329–337.

(30) Lin, X. S.; Zhang, G.; Ye, N. *Cryst. Growth Des.* **2009**, *9*, 1186–1189.
(31) Yao, J. Y.; Mei, D. J.; Bai, L.; Lin, Z. S.; Yin, W. L.; Fu, P. Z.; Wu, Y. C. *Inorg. Chem.* **2010**, *49*, 9212–9216.
(32) Pobedimskaia, E. A.; Alimova, L. L.; Belov, N. V.; Badikov, V. V. *Dokl. Akad. Nauk SSSR* **1981**, *257*, 611–614.
(33) Das, S.; Ghosh, C.; Gangopadhyay, S.; Andreev, Y. M.; Badikov, V. V. *Jpn. J. Appl. Phys.* **2006**, *45*, 5795–5797.
(34) Petrov, V.; Badikov, V.; Shevyrdyaeva, G.; Panyutin, V.; Chizhikov, V. *Opt. Mater.* **2004**, *26*, 217–222.
(35) Kim, Y.; Seo, I. S.; Martin, S. W.; Baek, J.; Halasyamani, P. S.; Arumugam, N.; Steinfink, H. *Chem. Mater.* **2008**, *20*, 6048–6052.
(36) Bera, T. K.; Song, J. H.; Freeman, A. J.; Jang, J. I.; Ketterson, J. B.; Kanatzidis, M. G. *Angew. Chem., Int. Ed.* **2008**, *47*, 7828–7832.
(37) Banerjee, S.; Malliakas, C. D.; Jang, J. I.; Ketterson, J. B.; Kanatzidis, M. G. *J. Am. Chem. Soc.* **2008**, *130*, 12270–12272.
(38) Chung, I.; Song, J.-H.; Jang, J. I.; Freeman, A. J.; Ketterson, J. B.; Kanatzidis, M. G. *J. Am. Chem. Soc.* **2009**, *131*, 2647–2656.
(39) Liao, J. H.; Marking, G. M.; Hsu, K. F.; Matsushita, Y.; Ewbank, M. D.; Borwick, R.; Cunningham, P.; Rosker, M. J.; Kanatzidis, M. G. *J. Am. Chem. Soc.* **2003**, *125*, 9484–9493.
(40) Sheldrick, G. M. *SHELXL-97*; University of Göttingen: Göttingen, Germany, 1997.
(41) Spek, A. L. *J. Appl. Crystallogr.* **2003**, *36*, 7–13.
(42) Wendlandt, W. W.; Hecht, H. G. *Reflectance Spectroscopy*; Interscience: New York, 1966.
(43) Kurtz, S. K.; Perry, T. T. *J. Appl. Phys.* **1968**, *39*, 3798–3813.
(44) Clark, S. J.; Segall, M. D.; Pickard, C. J.; Hasnip, P. J.; Probert, M. J.; Refson, K.; Payne, M. C. *Z. Kristallogr.* **2005**, *220*, 567–570.
(45) Payne, M. C.; Teter, M. P.; Allan, D. C.; Arias, T. A.; Joannopoulos, J. D. *Rev. Mod. Phys.* **1992**, *64*, 1045–1097.
(46) Perdew, J. P.; Burke, K.; Ernzerhof, M. *Phys. Rev. Lett.* **1996**, *77*, 3865–3868.
(47) Pack, J. D.; Monkhorst, H. J. *Phys. Rev. B* **1977**, *16*, 1748–1749.
(48) Geng, L.; Cheng, W.-D.; Zhang, H.; Lin, C.-S.; Zhang, W.-L.; Li, Y.-Y.; He, Z.-Z. *Inorg. Chem.* **2011**, *50*, 2378–2384.
(49) Brown, I. D.; Altermatt, D. *Acta Crystallogr., Sect. B* **1985**, *41*, 244–247.
(50) Brese, N. E.; O'keeffe, M. *Acta Crystallogr., Sect. B* **1991**, *47*, 192–197.
(51) Payne, D. J.; Egdell, R. G.; Walsh, A.; Watson, G. W.; Guo, J.; Glans, P. A.; Learmonth, T.; Smith, K. E. *Phys. Rev. Lett.* **2006**, *96*, 157403–157406.
(52) Yang, J.; Dolg, M. *Phys. Chem. Chem. Phys.* **2007**, *9*, 2094–2102.
(53) Kresse, G.; Furthmüller, J. *Phys. Rev. B* **1996**, *54*, 11169–11186.
(54) Kresse, G.; Furthmüller, J. *Comput. Mater. Sci.* **1996**, *6*, 15–50.
(55) Kresse, G.; Joubert, D. *Phys. Rev. B* **1999**, *59*, 1758–1775.